IOP PUBLISHING NANOTECHNOLOGY
Nanotechnology **18** (2007) 375706 (8pp) doi:10.1088/0957-4484/18/37/375706

A membrane–spring model for carbon nanotubes with van der Waals interaction between non-bonded atoms

Min Wang, Xiong Zhang, QuanShui Zheng and Yan Liu

Department of Engineering Mechanics, Tsinghua University, Beijing 100084, People's Republic of China

E-mail: xzhang@tsinghua.edu.cn

Received 30 April 2007, in final form 29 June 2007
Published 22 August 2007
Online at stacks.iop.org/Nano/18/375706

Abstract
The membrane–spring model was proposed by the authors to simulate the nonlinear mechanical responses of single-walled carbon nanotubes (CNTs). In order to investigate the complex behavior of multi-walled CNTs or CNT related structures, the van der Waals interaction between the non-bonded atoms should be included. In this paper, the van der Waals interaction is introduced into the membrane–spring model by using the atomic integration method. The nonlinear interaction is calculated at the atomic level, and then mapped to nodes. Consequently, the equations of motion are solved on nodes instead of atoms. The nonlinear deformations of single- and multi-walled CNTs are investigated by using the proposed model.

(Some figures in this article are in colour only in the electronic version)

1. Introduction

Numerical simulation plays an important role in exploring the properties of carbon nanotubes (CNTs) due to the difficulty of experiments on such tiny and complex structures. By using atomic methods including *ab initio* and molecular dynamics (MD), the fundamental physical properties of CNTs have been investigated [1–4], and important prospective applications have been explored or validated [5, 6]. However, owing to the huge calculations required for the atomic methods, the space and time scale of objects analyzed are limited. Some continuum or quasi-continuum models [7–13] have been proposed to explore the complex mechanical deformation of CNTs and CNT-related structures. These models have been used to analyze many problems, such as the rippling phenomena of bent nanotubes, the uniaxial compressed deformation of CNTs, and so on.

The van der Waals (vdW) interactions must be included in the analysis of multi-walled carbon nanotubes (MWNTs) or more complex system of CNTs. Several methods have been put forward to include the vdW effect in the continuum models. Liu [14] proposed the shell–cobweb model, in which nonlinear springs were initially set between nodes of shell elements instead of the vdW interaction between atoms. In their work, a set of atoms was assumed to be centralized on nodes in the neighborhood, which would result in errors when the meshing of elements was coarse. Pantano *et al* [10] used an interaction element to simulate the vdW force. The wall-to-wall shear resistance was ignored in their model, so it was unable to model the CNTs' behavior where the wall-to-wall shear effect was dominant. In the work of Li and Chou [15], the vdW effect between atoms was modeled by a truss rod. In their analysis, there were as many nodes of elements as atoms. Additionally, the effect of the vdW interaction on the uniaxial compression has been examined in detail through theoretical analysis [16, 17].

The membrane–spring model was proposed in our previous work [13] to simulate the nonlinear mechanical responses of single-walled carbon nanotubes (SWNTs). In this paper, the atomic integration method is proposed to introduce the vdW interaction into the membrane–spring model to model the MWNTs and CNT-related structures. The atoms are embedded in the membrane elements at their exact position, and deform together with the membranes. The vdW forces between atoms are calculated in the same way as in the MD method, and then mapped to the related nodes. In this method, the properties of the vdW interaction at the atomic level are maintained, such as the long-range interaction and the strong

 © 2007 IOP Publishing Ltd Printed in the UK

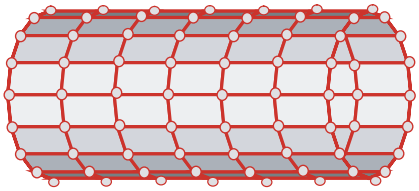

Figure 1. An SWNT is modeled by the membrane–spring model. In the figure, solid lines are springs, squares enclosed by lines are membranes, and hollow circles are finite element nodes.

nonlinear property depending on the atoms' distance. The total number of degrees of freedom depends on the number of nodes instead of atoms. Therefore, the membrane–spring model with vdW interaction is an efficient method for simulating the complex mechanical behavior of CNTs or CNT-related structures.

2. The membrane–spring model

The membrane–spring model [13] was proposed for the single-atom sheet structure of an SWNT or a graphite sheet. An SWNT or a single graphite sheet was modeled as a number of membranes connected by rotational springs, as shown in figure 1. The membrane models the in-plane behavior while the spring displays the bending resistance.

The mechanical properties of membranes are the same as those of a monolayer graphite sheet. The well-known linear elastic matrix of graphite [18] is

$$\boldsymbol{D} = \begin{bmatrix} 1060 & 180 & 15 & 0 & 0 & 0 \\ 180 & 1060 & 15 & 0 & 0 & 0 \\ 15 & 15 & 36.5 & 0 & 0 & 0 \\ 0 & 0 & 0 & 4.5 & 0 & 0 \\ 0 & 0 & 0 & 0 & 4.5 & 0 \\ 0 & 0 & 0 & 0 & 0 & 440 \end{bmatrix} \text{GPa} \quad (1)$$

if the graphite sheet plane is parallel to the x–y plane. Note that the interplanar spacing of graphite sheets $h = 0.34$ nm has been taken as the thickness of a single-layer graphite sheet in equation (1), so that the in-plane behavior of a single-layer graphite sheet can be modeled as

$$\boldsymbol{N} = \boldsymbol{D}_{\mathrm{m}}\boldsymbol{\varepsilon}, \quad (2)$$

where $\boldsymbol{N} = [\, N_x \quad N_y \quad N_{xy} \,]^{\mathrm{T}} = [\, h\sigma_x \quad h\sigma_y \quad h\sigma_{xy} \,]^{\mathrm{T}}$ is the internal force, $\boldsymbol{\varepsilon} = [\, \varepsilon_x \quad \varepsilon_y \quad \varepsilon_{xy} \,]^{\mathrm{T}}$ is the strain, and the in-plane stiffness matrix is

$$\boldsymbol{D}_{\mathrm{m}} = \begin{bmatrix} 360.4 & 61.2 & 0 \\ 61.2 & 360.4 & 0 \\ 0 & 0 & 149.6 \end{bmatrix} \text{N m}^{-1}. \quad (3)$$

It can be seen from the matrix (3) that the material property of the membranes in the x–y plane is assumed to be isotropic. The strain energy of the membrane elements is

$$V_{\mathrm{m}} = \sum_{i=1}^{n_{\mathrm{m}}} \int_{A_i} \tfrac{1}{2}\boldsymbol{N}^{\mathrm{T}}\boldsymbol{\varepsilon}\,\mathrm{d}A = \sum_{i=1}^{n_{\mathrm{m}}} \int_{A_i} \tfrac{1}{2}\boldsymbol{\varepsilon}^{\mathrm{T}}\boldsymbol{D}_{\mathrm{m}}\boldsymbol{\varepsilon}\,\mathrm{d}A \quad (4)$$

where n_{m} is the number of membrane elements.

In the simulation, the total deformation is divided into many time steps. In every time step, the configuration in the last step is taken as the reference configuration. $\boldsymbol{\varepsilon}_n$ is defined as the initial strain matrix of membranes in the reference configuration (at the time step n). In a single time step (from step n to $n+1$), vector $\Delta\boldsymbol{u}_e$ is the incremental displacement vector of a point in a membrane element in its local coordinate system, and $\Delta\boldsymbol{u}$ is the incremental nodal displacement vector of the element in the global coordinate system. They have the relationship $\Delta\boldsymbol{u}_e = \boldsymbol{R}\boldsymbol{N}\Delta\boldsymbol{u} = \bar{\boldsymbol{N}}\Delta\boldsymbol{u}$, where $\boldsymbol{R}$ is the transition matrix from the global coordinate system to the local one, $\boldsymbol{N}$ is the typical shape function in the finite element method, and $\bar{\boldsymbol{N}} = \boldsymbol{R}\boldsymbol{N}$. Consequently, the deformation of membranes at the current configuration (at the time step $n+1$) is given as

$$\boldsymbol{\varepsilon}_{n+1} = \boldsymbol{\varepsilon}_n + \boldsymbol{L}\Delta\boldsymbol{u}_e = \boldsymbol{\varepsilon}_n + \boldsymbol{L}\bar{\boldsymbol{N}}\Delta\boldsymbol{u} \quad (5)$$

where $\boldsymbol{L}$ is the differential operator of the membranes. Substituting equation (5) into (4), the stain energy of membranes is rewritten as

$$\begin{aligned} V_{\mathrm{m}} &= \sum_{i=1}^{n_{\mathrm{m}}} \int_{A_i} \tfrac{1}{2}(\boldsymbol{\varepsilon}_n + \boldsymbol{L}\bar{\boldsymbol{N}}\Delta\boldsymbol{u})^{\mathrm{T}}\boldsymbol{D}_{\mathrm{m}}(\boldsymbol{\varepsilon}_n + \boldsymbol{L}\bar{\boldsymbol{N}}\Delta\boldsymbol{u})\,\mathrm{d}A \\ &= \sum_{i=1}^{n_{\mathrm{m}}} \left[\tfrac{1}{2}\Delta\boldsymbol{u}^{\mathrm{T}}\boldsymbol{K}_{\mathrm{m}_i}\Delta\boldsymbol{u} + \Delta\boldsymbol{u}^{\mathrm{T}}\boldsymbol{F}_{\mathrm{m}_i} + V_{\mathrm{m}_i}\right] \end{aligned} \quad (6)$$

where

$$\boldsymbol{K}_{\mathrm{m}_i} = \int_{A_i} (\bar{\boldsymbol{N}}^{\mathrm{T}}\boldsymbol{L}^{\mathrm{T}}\boldsymbol{D}_{\mathrm{m}}\boldsymbol{L}\bar{\boldsymbol{N}})\,\mathrm{d}A \quad (7)$$

$$\boldsymbol{F}_{\mathrm{m}_i} = \int_{A_i} (\bar{\boldsymbol{N}}^{\mathrm{T}}\boldsymbol{L}^{\mathrm{T}}\boldsymbol{D}_{\mathrm{m}}\boldsymbol{\varepsilon}_n)\,\mathrm{d}A \quad (8)$$

$$V_{\mathrm{m}_i} = \int_{A_i} \left(\tfrac{1}{2}\boldsymbol{\varepsilon}_n^{\mathrm{T}}\boldsymbol{D}_{\mathrm{m}}\boldsymbol{\varepsilon}_n\right)\mathrm{d}A \quad (9)$$

$\boldsymbol{K}_{\mathrm{m}_i}$, $\boldsymbol{F}_{\mathrm{m}_i}$, and V_{m_i} are the stiffness matrix of membranes, the internal stress vector of membranes, and the strain energy of membranes in the reference configuration, respectively.

The stiffness of springs is obtained from the energy equivalence between the potential energies of the atomic calculation and the strain energies of rational springs in the wrapping process from graphite sheets into CNTs. Robertson *et al* [19] compared the energies of SWNTs with various radii with a graphite sheet, using both empirical potentials and first-principles total-energy methods. They found that the strain energy per carbon atom relative to an unstrained graphite sheet varies as $1/r^2$. According to the energy equivalence between the potential energies of atoms and the strain energies of springs, the stiffness of springs k_e can be obtained [13]. In the membrane–spring model, the rotation of springs can be determined in terms of the displacements of their adjacent membranes. The relation $\theta_{n+1} = \theta_n + \boldsymbol{B}\Delta\boldsymbol{u}$ can be obtained [13], where θ_n and θ_{n+1} are the angles of springs in the reference and current configurations, and $\boldsymbol{B}$ is the relational matrix between the incremental displacement of springs and those of the membranes' nodes. Consequently, the strain energy of the springs is

$$\begin{aligned} V_{\mathrm{s}} &= \sum_{e=1}^{n_{\mathrm{s}}} \tfrac{1}{2}k_e[\theta_n + \boldsymbol{B}\Delta\boldsymbol{u}]^2 \\ &= \sum_{e=1}^{n_{\mathrm{s}}} \left[\tfrac{1}{2}\Delta\boldsymbol{u}^{\mathrm{T}}\boldsymbol{K}_{\mathrm{s}_e}\Delta\boldsymbol{u} + \Delta\boldsymbol{u}^{\mathrm{T}}\boldsymbol{F}_{\mathrm{s}_e} + \tfrac{1}{2}k_e\theta_n^2\right] \end{aligned} \quad (10)$$

where n_s is the number of springs. $\boldsymbol{K}_{s_e} = k_e \boldsymbol{B}^T \boldsymbol{B}$ is the stiffness matrix of the springs, and $\boldsymbol{F}_{s_e} = k_e \theta_n \boldsymbol{B}^T$ the internal stress vector of the springs.

Combining membranes with springs, the total energy of the membrane–spring model is

$$V = V_m + V_s \tag{11}$$

Consequently, the equilibrium equation for the membrane–spring model is

$$\frac{\partial V}{\partial \Delta \boldsymbol{u}} = \boldsymbol{P}, \tag{12}$$

where $\boldsymbol{P}$ is the external applied load. Substituting the expression in equations (6) and (10), the equilibrium equation (12) is rewritten as

$$\sum_{i=1}^{n_m} (\boldsymbol{K}_{m_i} \Delta \boldsymbol{u} + \boldsymbol{F}_{m_i}) + \sum_{e=1}^{n_s} (\boldsymbol{K}_{s_e} \Delta \boldsymbol{u} + \boldsymbol{F}_{s_e}) = \boldsymbol{P}. \tag{13}$$

It was reported that the relation between the strain energy of an SWNT relative to an unstrained graphite sheet and the radius r is insensitive to other aspects of the lattice structure. This means that the wrapping process of SWNTs does not depend on the chirality. From the above discussion, it can be seen that the deformation of graphite sheets in their plane is isotropic. Therefore, the chirality of SWNTs has no effect on the membrane–spring model without vdW interaction.

3. The atomic integration method for vdW interaction

The vdW interaction acts between non-bonded pairs of atoms, and it is a strong nonlinear interaction subject to the distance of the atom pairs. Generally, the vdW energy can be described in two types of expression, namely, the Lennard-Jones (LJ) potential and the Morse-type potential. The classical LJ potential [20] is given as

$$U_{vdw} = A \left(\frac{1}{2} \frac{r_0^6}{r^{12}} - \frac{1}{r^6} \right) \tag{14}$$

with the parameters $r_0 = 0.3834$ nm and $A = 24.3 \times 10^{-25}$ J(nm)^6. In equation (14), r is the distance between the atom pair. The Morse-type potential obtained on the basis of a local density approximation calculation [21] can be expressed as

$$U_{vdw} = D_e[(1 - e^{-\beta(r-r_e)})^2 - 1] + E_r e^{-\beta' r} \tag{15}$$

where $D_e = 6.50 \times 10^{-3}$ eV is the equilibrium binding energy, $E_r = 6.94 \times 10^{-3}$ eV is the hard-core repulsion energy, $r_e = 0.405$ nm, $\beta = 10.0$ nm^{-1}, and $\beta' = 40.0$ nm^{-1}.

Qian *et al* [22] analyzed two types of expressions, and compared them with the published experimental data and the result of the *ab initio* method. They concluded that the LJ expression was appropriate for the vdW potential in the attractive range while the Morse type was relatively close to the experimental results in the repulsive one. Therefore, a combined formation was proposed for the vdW interaction. When the distance between non-bonded atoms is less than 0.33 nm, the Morse-type potential was applied; the LJ potential is used if the distance is larger than 0.34 nm; and in the transition region from 0.33 to 0.34 nm, an interpolation is carried out to ensure the continuity of the potential and force. In most of the following simulations, this combined formation (named the LM potential) with the cutoff range from 0.2 to 1.13 nm is adopted to calculate the vdW force between atoms not only located on different walls, but also on the same wall.

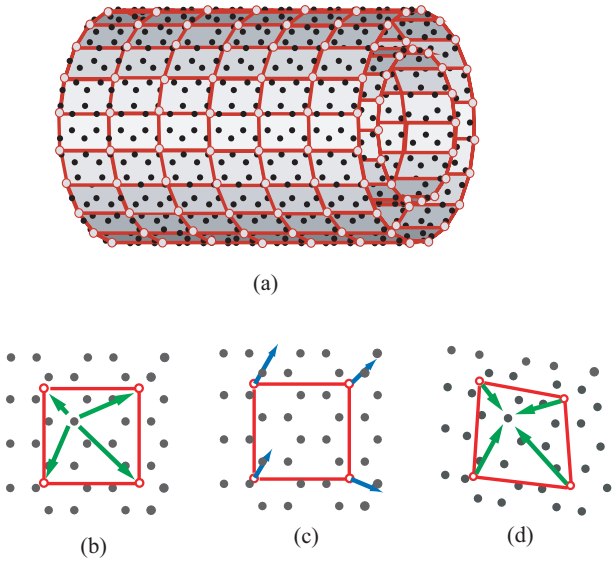

Figure 2. (a) An MWNT is modeled by the membrane–spring model with vdW interaction. (b)–(d) schematic illustration of the atomic integration method: (b) mapping the vdW force from atoms to nodes; (c) solving nodal velocities and displacements; (d) updating the position of atoms on the basis of nodal displacements. In this figure, solid circles are atoms.

The vdW force $\boldsymbol{F}_i$ exerted on atom i can be easily determined from the potential energy U_{vdw} as

$$\boldsymbol{F}_i = \sum_{\forall j} \left(-\frac{\partial U_{vdw}}{\partial \boldsymbol{r}_{ij}} \right) \tag{16}$$

where $\boldsymbol{r}_{ij} = \boldsymbol{r}_i - \boldsymbol{r}_j$, $\boldsymbol{r}_i$ and $\boldsymbol{r}_j$ are the displacement vectors of atom i and j.

In the membrane–spring model, the equations of motion are established on nodes of membranes. In order to include the nonlinear vdW interaction and keep the number of degrees of freedom constant, the atomic integration method is proposed. In this approach, atoms are assumed to be attached to membranes as shown in figure 2(a); they deform with the elements in the same manner. The vdW forces on atoms are mapped to nodes according to the relationship of atoms and nodes, and the force on nodes can be considered as the external applied load to be included into the solving equation. The process in every time step is described in detail, as shown in figures 2(b)–(d). The vdW forces on atoms are calculated according to the current position of the atoms, and they are mapped to the nodes as shown in figure 2(b). Together with the contribution of membranes and springs, the nodal displacements and velocities are calculated from the equations of motion as illustrated in figure 2(c). The positions of the atoms are updated in the same manner as the nodal displacements, as shown in figure 2(d).

In the numerical calculation, the position vector of atom i, $\boldsymbol{r}_i$, can be determined by

$$\boldsymbol{r}_i = \sum_{J=1}^{n} N_{Ji}\boldsymbol{r}_J \tag{17}$$

where N_{Ji} is the typical finite element shape function of node J evaluated at atom i, and $\boldsymbol{r}_J$ is the position vector of node J. n is the number of nodes in the membrane element that the atom i resides in, which equals three for triangular elements, and four for quadranglular elements. The relationship between atoms and elements can be determined as the meshing of elements is set. The finite element shape function N_{Ji} is given by

$$N_{Ji} = A_{Ji}/A \tag{18}$$

for triangle elements, and given by

$$N_{Ji} = \tfrac{1}{4}(1 + \xi_J\xi_i)(1 + \eta_J\eta_i) \tag{19}$$

for quadranglular elements. In equation (18), A is the area of the membrane element that the atom i resides in, and A_{Ji} is the Jth area coordinate of atom i. In equation (19), ξ_i and η_i are the normalized coordinates of atom i, so ξ_J and η_J take on their nodal values of $(\pm 1, \pm 1)$ at the nodes.

The force vector of node J due to the vdW interaction is obtained by

$$\boldsymbol{F}_{\mathrm{vdw}_J} = \sum_{e}^{n_J}\sum_{i=1}^{n_e} N_{Ji}\boldsymbol{F}_i \tag{20}$$

where $\boldsymbol{F}_{\mathrm{vdw}_J}$ is the force vector of node J, n_J is the number of elements connected to node J, and n_e is the number of atoms residing in element e. This procedure is termed as the atomic integration in this paper, because the calculation of equation (20) is similar to the numerical integration in the finite element method. In this method, the vdW interaction is calculated in the same way as that in the MD method. However, the mapping procedure in equation (20) smoothes the atomic force, which is of great benefit to the stability of the time integrator because the high-frequency components are filtered out from the response.

In this way, the vdW interaction is included into the membrane–spring model. On adding the vdW force on nodes as in equation (20) into (13), the equilibrium equation is rewritten as

$$\sum_{i=1}^{n_\mathrm{m}}(\boldsymbol{K}_{\mathrm{m}_i}\Delta\boldsymbol{u} + \boldsymbol{F}_{\mathrm{m}_i}) + \sum_{e=1}^{n_\mathrm{s}}(\boldsymbol{K}_{\mathrm{s}_e}\Delta\boldsymbol{u} + \boldsymbol{F}_{\mathrm{s}_e}) = \boldsymbol{P} + \sum_{J=1}^{n_\mathrm{n}}\boldsymbol{F}_{\mathrm{vdw}_J} \tag{21}$$

where n_n is the number of nodes in the simulation. Using the membrane–spring model with vdW interaction, both the small and large deformation mechanical responses of CNTs and their related structures can be analyzed. In the following sections, the nonlinear deformations of SWNTs and MWNTs are simulated, and compared with other methods.

4. The complex deformation of CNTs

4.1. Buckling of SWNTs subject to radial compression

It has been reported that the diameters of SWNTs are mostly dispersed in the range 0.7–3.0 nm with a peak at 1.7 nm [23]. Those with larger diameters were found in flattened configurations or even could not exist stably due to vdW attraction. Chopra *et al* [24] first discovered the fully collapsed CNT in experiments, and explained the phenomenon in theoretical analysis. Using the MD method, Gao *et al* [25] explored the stability of SWNTs in the radial direction through comparing the circular and collapsed cross section configurations of SWNTs. They provided two tradeoff radii, $R_1 = 1.0$ nm and $R_2 = 3.0$ nm. For SWNTs with radius below R_1, only the circular configurations can exist, while for those with radius larger than R_2, the collapsed ones are stable. For SWNTs with radius between the two critical values, the collapsed configurations can exist but they are only metastable because the circular ones are energetically favorable.

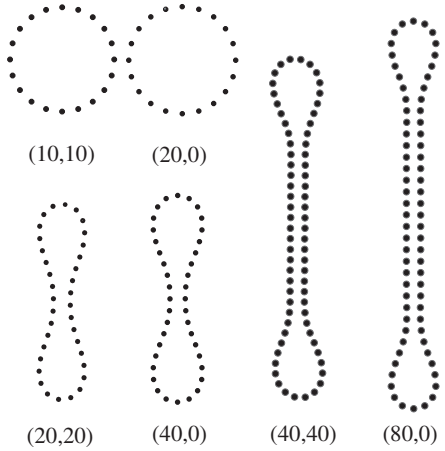

Figure 3. The final relaxed configurations of tubes' cross sections. The dots in the figure are nodes rather than atoms.

In an actual situation, SWNTs usually contact with the substrate or other CNTs, which may promote the buckling phenomenon. Therefore, a difference of critical radii existed between the experimental and the MD simulation results [25]. For simplicity, the interaction of SWNTs with the substrate or other CNTs is also omitted in the following analysis. Individual zigzag SWNTs (20, 0), (40, 0), (80, 0) and armchair SWNTs (10, 10), (20, 20), (40, 40) with the length of about 10.0 nm are examined, respectively. A circular tube is first relaxed without any constraint, and then the displacement load is applied on the two opposite sides to squeeze the tube. When the space between the opposite faces is as little as 0.34 nm, the load is withdrawn and the tube is fully relaxed. Figure 3 displays the final cross section configurations of the SWNTs. It can be seen that tubes (20, 0) and (10, 10), whose radii are less than 1.0 nm, revert to the circular configurations when the load is withdrawn, while the others become collapsed ones. By measuring the collapsed configurations, it can be obtained that the inner wall distances in the flattened region are 0.330–0.337 nm and the maximum distances between the elliptical ends are about 1.04–1.08 nm. It should be noted that the sections in figure 3 are those of tubes at the height of 5.0 nm. The sections at the two ends have values slightly larger than those at the middle height due to the boundary effect, but the difference is less than 2%. These results agree well with those obtained by the MD method [25], which are about 0.34 and 1.05 nm, respectively.

Table 1 presents the equilibrium energies per atom for SWNTs with circular and collapsed cross sections. It can

Table 1. The total energy per atom for circular and collapsed configurations, including the strain energy of the membrane–spring and the vdW potential.

(n, m)	Radius (nm)	Circular (10^{-20} J)	Collapsed (10^{-20} J)
(20, 20)	1.357	4.634	4.843
(40, 0)	1.567	4.613	4.795
(40, 40)	2.714	4.520	4.518
(80, 0)	3.134	4.520	4.488

be found that the collapsed form is energetically favorable for SWNTs (80, 0) and (40, 40), while the collapsed form of SWNTs (40, 0) and (20, 20) has a higher energy than the circular form, which means their collapsed configurations are metastable. There is a very slight difference between values (4.520 and 4.518) for SWNT (40, 40). It can be predicted that the cutoff radius of R_2 is close to 2.7 nm, a little smaller than the value of 3.0 nm in Gao's analysis [25].

The 3D configurations of collapsed tubes (40, 40) and (80, 0) are shown in figure 4(a). Apparently, the collapsed tube (40, 40) is straight and has a nearly uniform deformation along the axial direction. However, for tube (80, 0), the axial displacement of one side is larger than the other one, implying that the end section is not in the same plane. The cross sections at different heights, including the top, middle and bottom ones, are illustrated in figure 4(b). The difference in cross sections is also observed between the armchair and zigzag tube. Tube (40, 40) has nearly the same sectional shapes at different heights, while the top and bottom sections of tube (80, 0) deflect to reverse sides. The difference between the armchair and zigzag tubes is mainly due to the effect of interlayer lattice registry existing in the flattened region. Liu *et al* [26] analyzed the effect of interlayer lattice registry on the formation of fully collapsed SWNTs, and reported that this effect resulted in the varied morphologies of the straight, warping and twisted ribbons. The effect of interlayer lattice registry existing in our model is not so obvious compared with the atomic method because of the smooth process of mapping.

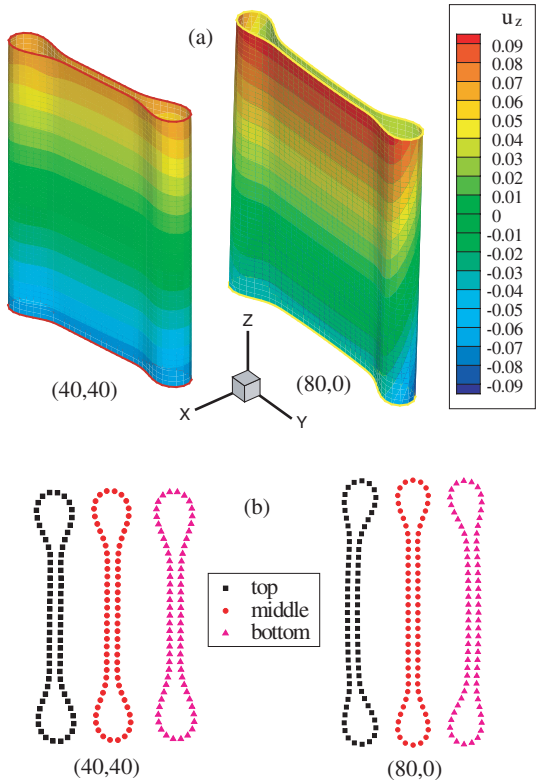

Figure 4. (a) The 3D configurations of collapsed tubes and their displacement in the axial direction described in the contour. Tube (40, 40) is straight and has uniform deformation along axis, while tube (80, 0) has a slight difference between the opposite faces of the flattened region. (b) The cross section configurations of the collapsed tubes at the top, middle, and bottom. Tube (40, 40) has nearly the same sections at different heights, while the top and bottom sections of tube (80, 0) deflect to reverse sides.

4.2. Pure bending of CNTs

The kink structures of bent CNTs were observed in the experiments of Iijima [3], and this deformation was simulated by the MD method [2, 3]. The single nanotubes examined could be bent to large angles, and it was found that the tube was completely reversible even when the bending angle was larger than 110° [3]. The equation for the critical curvature C_c was obtained through the results of several SWNTs examined by Iijima [3], and is expressed as

$$C_c = \frac{1.49}{d^2}\left[1 + \frac{9.89}{d^5}10^3\cos(6h)\right] \qquad (22)$$

where d is the tube's diameter in units of Å, and h represents the helicities. $h = 0$ is for zigzag tubes and $h = \pi/6$ for armchair tubes. Yakobson *et al* [2] obtained a similar conclusion. Additionally, methods based on the continuum or quasi-continuum theory, such as the membrane model [8] and the shell model [10], were also used to examine the bending deformation of SWNTs, and the results were in agreement with the atomic simulation in the elastic range.

In this example, an SWNT (9, 9) with a diameter of 1.2 nm is examined for bending deformation. When it is fully relaxed, the tube's ends are constrained on their own rigid surfaces, respectively. The surfaces are rotated in steps, and the tube is bent in the same manner. The total energy increases smoothly with the increase of applied bending angle. At the critical bending angle of 40.0° (0.7 rad), the tube buckles sideways as a whole to form a kink structure. At the same time, the total energy drops suddenly, as shown in figure 5(a). The tube has a length of 9.0 nm; consequently the corresponding critical curvature is about 0.078 rad nm^{-1}, which is little smaller than the MD result of 0.1 rad nm^{-1} [3]. By observing the detailed process of buckling, it can be found that the tube has the configuration shown in figure 5(b) just before forming the obvious kink structure at the center of the tube, as shown in figure 5(c). This process happens very quickly, and the two configurations occur at nearly the same bending angle. Until the bending angle of 1.0 rad is applied, one kink structure is maintained and the total energy increases linearly.

By inserting a SWNT (4, 4) with the same length into the SWNT (9, 9), or adding a SWNT (14, 14) outside of the SWNT (9, 9), double-walled carbon nanotube (DWNTs) are formed. Multiple kinks occur when DWNTs are bent in a similar way, but some different phenomena occur on the two kinds of tube. For DWNT (9, 9)/(14, 14), the outer diameter is

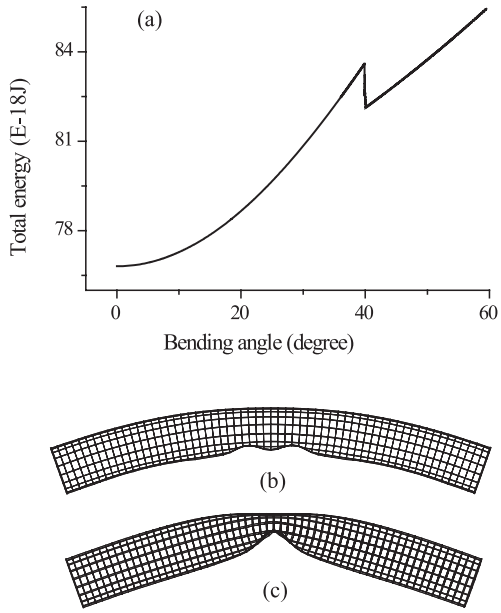

Figure 5. (a) Total energy changes with the bending angle, (b) the configuration of the tube beginning to buckle, and (c) the configuration of the kink structure when the buckling process has finished. The two configurations occur at nearly the same critical bending angle of 40.0°.

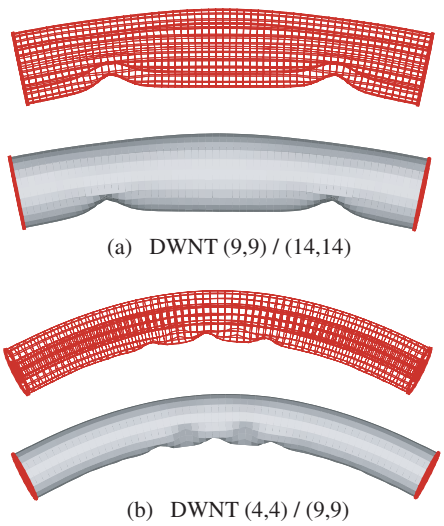

Figure 6. (a) The configurations of the kink structure for DWNT (9, 9)/(14, 14) at a bending angle of 22°, and (b) for DWNT (4, 4)/(9, 9) at a bending angle of 51.5°.

1.9 nm and the inner one is 1.2 nm, and there is relatively weak resistance along the radial direction. Two kinks form early at the bending angle of 22.0°, and the two walls have the same deformation, as shown in figure 6(a). DWNT (4, 4)/(9, 9) has the smaller inner diameter of 0.543 nm, and the kink structure occurs at the bending angle of 51.5°. A repulsive interaction exists between the opposite sides of the inner tube to prevent the kinks deepening, so there are more kinks on the tube, as shown in figure 6(b).

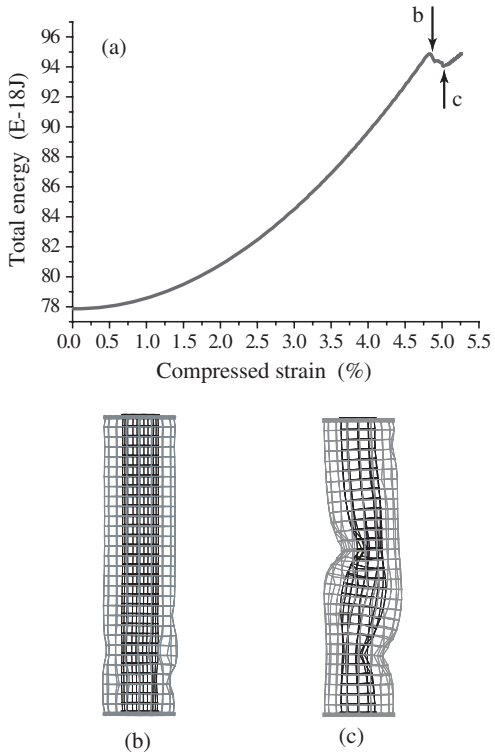

Figure 7. (a) Total energy of the DWNT versus the compressed strain. (b)–(c) configurations of tubes at $\varepsilon = 4.78\%$ and 5.0% labeled b and c in (a).

4.3. Deformation of MWNTs subject to axial compression

For an SWNT, the vdW interaction has little effect on the critical strain for buckling subject to the axial compression. For an MWNT, the walls with various radii interact with each other through the vdW interaction, so what happens to their critical strain under axial compression? In this example, DWNT (5, 5)/(10, 10) with a length of 6.0 nm is first examined. The DWNT is relaxed to obtain the stable configuration under the combined effect of the covalent bonds and the vdW interaction, and then one end is fully fixed while the other is compressed slowly along the axial direction. Figure 7(a) illustrates the variation of the total energy, including the strain energy of the membrane–spring and the potential of the vdW interaction for DWNT (5, 5)/(10, 10). The energy increases with the increase of the compressed strain ε until it reaches the critical value of 0.0478, which is indexed as b in figure 7(a), and then it drops suddenly because the outer straight tube begins to buckle. The change of the outer wall's shape alters its distance from the inner wall as well as the vdW force, which accelerates the buckling of the inner tube. The buckling finally finishes at $\varepsilon = 0.05$, which is indexed as c in the figure. Figures 7(b)–(c) shows the corresponding configurations at the strain of 0.0478 and 0.05, labeled b and c in figure 7(a). For SWNTs with a length of 6.0 nm, the critical strain of a (10, 10) tube is about 0.044 and that of a (5, 5) tube is close to 0.053. It can be seen that due to the vdW interaction, the critical strains of thin MWNTs subject to axial compression are slightly larger than those of SWNTs with the same radius of the MWNTs' outermost tube.

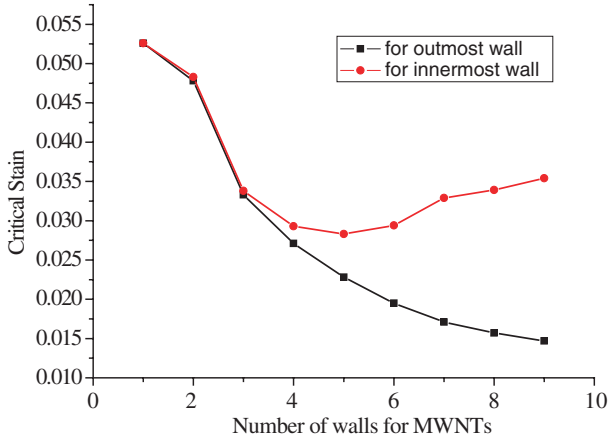

Figure 8. The critical strain of MWNTs with different walls when their outermost or innermost tubes enter into buckling.

A series of MWNTs, having the same innermost tubes (5, 5) and with the number of walls from two to nine, respectively, are obtained through adding the outside walls gradually. Those MWNTs, having the same length of 6.0 nm, are examined for their critical strain under axial compression. The curve with the square symbol in figure 8 is the axial strain of MWNTs when the outermost walls begin to buckling, while the curve with dots is the axial strain of MWNTs as the innermost tubes enter into buckling. It can be seen that all walls of MWNTs buckle simultaneously when the number of walls is small. The above analysis of DWNT (5, 5)/(10, 10) has explained the phenomena in detail. For MWNTs with the numbers of walls being larger than three, not all of the walls buckle at the same time, but the inner ones would keep their uniform axial deformation for a longer time. The radial deformation of MWNTs, due to the buckling of the outermost tube, is reduced by the vdW interaction between walls when the number of walls is large. Chang *et al* [27] theoretically discussed the size effect of the number of walls on the axial compression buckling phenomena, based on a molecular mechanics model, and obtained a similar conclusion.

4.4. Vibration of the DWNT

Owing to the low-friction between the walls of MWNTs, low-wear bearings [28] and gigahertz oscillators [29] have proposed, which would have profound implications on the application of CNTs, especially in nanoelectromechanical systems (NEMS). The wall-to-wall shear resistance is included in our proposed model so that it is capable of modeling low-wear bearings and gigahertz oscillators.

The object tube is a DWNT (5, 5)/(10, 10) with a length of 3.5 nm, and the radius difference between the inner and outer tube is about 0.339 nm. The vdW force that occurs in the same wall is ignored owing to the small deformation of the tubes, but the force that interacts between different walls is included. At first, the inner tube is slowly pulled out to a distance of 1.0 nm along its axis, while the outer tube is fully fixed. During the process of pulling out the inner tube, the vdW potential is increasing slowly, which is the retraction energy for vibration. After being released, the

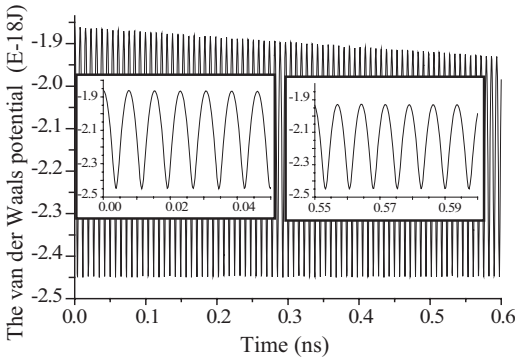

Figure 9. The vdW potential of the DWNT versus time. The inset figures are detailed ones for the first and last 0.05 ns of the vibration.

inner tube vibrates back and forth along the axial direction while the outer tube remains fixed. Figure 9 illustrates that the vdW potential varies periodically with the vibration, and the oscillation amplitude decreases slowly, which results in the decrease of the maximum extruding distance. According to the analysis of Zheng and Jiang [29], the frequency f and the extruded distance d have the relationship $f \propto 1/\sqrt{d}$; thus the frequency will also change with the vibration. From the inset figures in figure 9, the period, which is defined as the inner tube going from the leftmost position to the rightmost and back to the leftmost one, changes from 0.0154 to 0.0147 ns, while the frequency of vibration increases from 6.49×10^{10} to 6.80×10^{10} Hz.

In this simulation, the inner and outer tubes are all with open ends for the sake of convenience, which may create a difference with those with caps. The lump mass matrix used in our analysis will cause numerical damping, which increases the dissipation of energy. These factors would cause the difference with the analysis using MD [6]. The effects of temperature on the energy dissipation have not been considered yet in the membrane–spring model. Since temperature control is an important issue in energy dissipation [6], the rate of energy dissipation cannot be discussed yet. However, it can be concluded that the vibrations of CNTs have very high frequency, of the magnitude of gigahertz.

5. Conclusions

In this paper, the vdW interaction is introduced into the membrane–spring model through the atomic integration method. This method is efficient, and can be used to analyze the nonlinear deformation for SWNTs, MWNTs, tube–substrate interaction, and even for more complex cases. The numerical results obtained by the proposed model are in good agreement with those obtained by the MD and other methods, which validates the integrated membrane–spring model.

Acknowledgments

The authors gratefully acknowledge the financial support of the National Science Foundation of China through Grant No. 10672088, the National Basic Research Program of China through Grant No. 2004CB619304, and the Program for New Century Excellent Talents in Universities (NCET-04-0091).

References

[1] Dresselhaus M S, Dresselhaus G and Saito S 1995 *Carbon* **33** 883–91
[2] Yakobson B I, Brabec C J and Bernholc J 1996 *Phys. Rev. Lett.* **76** 2511–4
[3] Iijima S 1996 *J. Chem. Phys.* **104** 2089–92
[4] Zhou X, Zhou J J and Ou-Yang Z C 2000 *Phys. Rev.* B **62** 13692
[5] Hertel T, Walkup R E and Avouris P 1998 *Phys. Rev.* B **58** 13870–3
[6] Guo W L, Guo Y F, Gao H J, Zheng Q S and Zhong W Y 2003 *Phys. Rev. Lett.* **91** 125501
[7] Liu J Z, Zheng Q S and Jiang Q 2001 *Phys. Rev. Lett.* **86** 4843–6
[8] Arroyo M and Belytschko T 2002 *J. Mech. Phys. Solids* **50** 1941–77
[9] Li C Y and Chou T W 2003 *Int. J. Solids Struct.* **40** 2487–99
[10] Pantano A, Parks D M and Boyce M C 2004 *J. Mech. Phys. Solids* **52** 789–821
[11] Liu B, Huang Y, Jiang H, Qu S and Hwang K C 2004 *Comput. Methods Appl. Mech. Eng.* **193** 1849–64
[12] Wang L F, Zheng Q S, Liu J Z and Jiang Q 2005 *Phys. Rev. Lett.* **95** 105501
[13] Wang M, Zhang X and Lu M W 2005 *Phys. Rev.* B **72** 205403
[14] Liu J Z 2002 *PhD Thesis* Department of Engineering Mechanics, Tsinghua University
[15] Li C Y and Chou T W 2003 *Comput. Sci. Technol.* **63** 1517
[16] Ru C Q 2001 *J. Appl. Phys.* **89** 3426–33
[17] He X Q, Kitipornchai S and Liew K M 2005 *J. Mech. Phys. Solids* **53** 303–26
[18] Kelly B T 1981 *Physics of Graphite* (London: Applied Science)
[19] Robertson R H, Brenner D W and Mintmire J W 1992 *Phys. Rev.* B **45** 12592
[20] Girifalco C A and Lad R A 1956 *J. Chem. Phys.* **25** 693–7
[21] Wang Y, Tomanek D and Bertsch G F 1991 *Phys. Rev.* B **44** 6562–5
[22] Qian D, Liu W K and Ruoff R S 2001 *J. Phys. Chem.* B **105** 10753–8
[23] Dresselhaus M S, Dresselhaus G and Avouris P 2001 *Carbon Nanotubes Synthesis, Structure, Properties, and Applications* (Berlin: Springer)
[24] Chopra N G, Benedict L X, Crespi V H, Cohen M L, Louie S G and Zettl A 1995 *Nature* **377** 135–8
[25] Gao G H, Cagin T and Goddard W A III 1998 *Nanotechnology* **9** 184–91
[26] Liu B, Yu M F and Huang Y 2004 *Phys. Rev.* B **70** 161402(R)
[27] Chang T C, Guo W L and Guo X M 2005 *Phys. Rev.* B **72** 064101
[28] Cumings J and Zettl A 2000 *Science* **289** 602
[29] Zheng Q S and Jiang Q 2002 *Phys. Rev. Lett.* **88** 45503